



HAL
open science

On the origin of basal stacking faults in nonpolar wurtzite films epitaxially grown on sapphire substrates

Philippe Vennéguès, Jean Michel Chauveau, Z. Bougrioua, Tiankai Zhu, Denis Martin, Nicolas Grandjean

► To cite this version:

Philippe Vennéguès, Jean Michel Chauveau, Z. Bougrioua, Tiankai Zhu, Denis Martin, et al.. On the origin of basal stacking faults in nonpolar wurtzite films epitaxially grown on sapphire substrates. *Journal of Applied Physics*, 2012, 112 (11), pp.113518. 10.1063/1.4768686 . hal-02906733

HAL Id: hal-02906733

<https://hal.science/hal-02906733>

Submitted on 25 May 2022

HAL is a multi-disciplinary open access archive for the deposit and dissemination of scientific research documents, whether they are published or not. The documents may come from teaching and research institutions in France or abroad, or from public or private research centers.

L'archive ouverte pluridisciplinaire **HAL**, est destinée au dépôt et à la diffusion de documents scientifiques de niveau recherche, publiés ou non, émanant des établissements d'enseignement et de recherche français ou étrangers, des laboratoires publics ou privés.

On the origin of basal stacking faults in nonpolar wurtzite films epitaxially grown on sapphire substrates

Cite as: J. Appl. Phys. **112**, 113518 (2012); <https://doi.org/10.1063/1.4768686>

Submitted: 26 June 2012 • Accepted: 07 November 2012 • Published Online: 11 December 2012

P. Vennéguès, J. M. Chauveau, Z. Bougrioua, et al.



View Online



Export Citation



CrossMark

ARTICLES YOU MAY BE INTERESTED IN

[Luminescence from stacking faults in gallium nitride](#)

Applied Physics Letters **86**, 021908 (2005); <https://doi.org/10.1063/1.1852085>

[Imaging basal plane stacking faults and dislocations in \(11-22\) GaN using electron channelling contrast imaging](#)

Journal of Applied Physics **124**, 065301 (2018); <https://doi.org/10.1063/1.5042515>

[Intersecting basal plane and prismatic stacking fault structures and their formation mechanisms in GaN](#)

Journal of Applied Physics **98**, 063510 (2005); <https://doi.org/10.1063/1.2039278>

Lock-in Amplifiers
up to 600 MHz



Zurich
Instruments



On the origin of basal stacking faults in nonpolar wurtzite films epitaxially grown on sapphire substrates

P. Vennéguès,¹ J. M. Chauveau,^{1,2} Z. Bougrioua,³ T. Zhu,⁴ D. Martin,⁴ and N. Grandjean⁴

¹Centre de Recherche sur l'Hétéro-Epitaxie et ses Applications, Centre National de la Recherche Scientifique, CRHEA-CNRS, Rue Bernard Grégory, Sophia Antipolis, 06560 Valbonne, France

²University of Nice Sophia-Antipolis, Parc Valrose, 06103 Nice, France

³Institut d'Electronique de Microélectronique et de Nanotechnologie, CNRS and Lille University, 59652 Villeneuve d'Ascq, France

⁴Laboratory of Advanced Semiconductors for Photonics and Electronics, Institute of Condensed Matter Physics, Ecole Polytechnique Fédérale de Lausanne (EPFL), CH-1015 Lausanne, Switzerland

(Received 26 June 2012; accepted 7 November 2012; published online 11 December 2012)

The microstructure of nonpolar heteroepitaxial wurtzite films (GaN and ZnO-based) is dominated by the presence of planar basal stacking faults (BSFs). In this paper, transmission electron microscopy studies of both GaN and ZnO nonpolar films oriented either (11–20) or (1–100) and grown on sapphire substrates, permit to propose and evaluate different mechanisms of BSFs formation. The main mechanism of formation of BSFs results from a Volmer Weber growth mode. The first stage of the growth is a 3D nucleation. The 3D nuclei are relaxed at least along one in-plane orientation. BSFs are created in the coalescence boundaries in order to compensate translations between neighbouring islands. BSFs are well adapted to compensate in-plane translations in the case of nonpolar films. In fact, their plane is perpendicular to the substrate surface and this orientation is similar to the orientation of the coalescence boundaries. Moreover, their displacement vector has a component parallel to the translation between islands and their formation energy is low. On the other hand, in the case of the polar growth, BSFs are not adapted to compensate in-plane translation as their plane is perpendicular to the coalescence boundaries.

© 2012 American Institute of Physics. [<http://dx.doi.org/10.1063/1.4768686>]

I. INTRODUCTION

The hexagonal wurtzite structure which is the structure of wide band gap GaN- and ZnO-based semiconductors is polar, i.e., compatible with the existence of a spontaneous polarization.¹ The combined effects of this spontaneous polarization and of a possible piezoelectric polarization on the properties of heterostructures are maximal when the growth is performed along the polar c-axis. A lot of efforts have therefore been done in the last ten years to develop the growth along nonpolar directions (with the polar c-direction in the growth plane) so that the effects of internal polarizations are avoided. Very good material properties are today obtained with homoepitaxial layers and GaN-based highly efficient optoelectronic devices have already been fabricated.² However, the sizes of ZnO and mainly of GaN substrates remain small and heteroepitaxy has to be considered. Up to now, heteroepitaxially grown nonpolar wurtzite semiconductor films, either GaN- or ZnO-based, contain a high density of structural defects which prevent their use for the fabrication of efficient devices. These defects are mainly basal stacking faults (BSFs) which are terminated by partial dislocations (PDs) or connected to other BSFs by prismatic stacking faults (PSFs). The presence of numerous BSFs has been reported for all the substrates: for GaN films grown on 4H³- and 6H⁴-nonpolar SiC substrates, (1-102) R-sapphire^{5,6} and (100)-LiAlO₂⁷ and for ZnO films grown on R-sapphire^{8,9} and (1-102) R-LiTaO₃.¹⁰ The presence of these defects also seems to be independent of the growth method.

The origin of structural defects in any heteroepitaxially grown film is related to differences between the substrate and the deposited films in terms of structure, chemistry, lattice parameters and thermal expansion coefficients. For the above-cited hetero-substrates, different situations have to be considered. In both hexagonal SiC and wurtzite materials (GaN or ZnO) atoms are tetrahedrally coordinated with one cation–anion bond parallel to the [0001] direction. The structural difference is the stacking period of the hexagonal basal planes: 4 and 6 for 4H- and 6H-SiC and 2 for the wurtzite structure. The lattice mismatches are also low.¹¹ Therefore, 4H-SiC, 6H-SiC, and wurtzite GaN and ZnO have very close structures. Nevertheless, the densities of BSFs and related defects are very high in heteroepitaxial GaN films on nonpolar SiC substrates. The origin of these BSFs is attributed to an intrinsic property of epitaxial growth: the deposited films tend to adopt the structure of the substrate. In fact, BSFs in the wurtzite structure may be considered as inclusion of 4H or 6H stackings in the 2H wurtzite structure.¹¹ The other above-cited hetero-substrates (i.e., sapphire, LiAlO₂, and LiTaO₃) have structures which are entirely different from the wurtzite structure. The presence of structural defects in films deposited on such substrates is therefore expected. However, it is the nature of the defects which might be surprising. Sapphire substrates are the mostly used substrates for the heteroepitaxial growth of wurtzite materials be it for polar, nonpolar or semipolar (inclined c-axis) orientations. In the case of polar films grown on C-sapphire, the microstructure is dominated by the presence of vertical

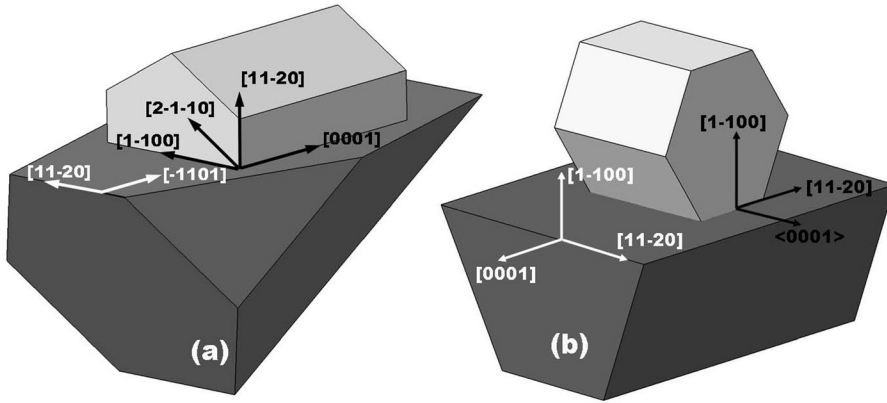


FIG. 1. Schematic representation of the epitaxial relationships between wurtzite nonpolar films with R-sapphire (a) and M-sapphire (b). The sapphire axes are in white and the GaN/ZnO axes in black.

perfect dislocations with, in the case of GaN, BSFs only in the nucleation layers grown at low temperature. The first objective of the present paper is to propose different mechanisms for the formation of BSFs observed in nonpolar GaN and ZnO films grown on R- and M-sapphire and to evaluate them, thanks to a transmission electron microscopy (TEM) study. A second objective is to understand the difference of the nature of defects from those observed in polar films grown on C-sapphire.

II. EXPERIMENTAL PROCEDURES

Three kinds of nonpolar wurtzite heteroepitaxial films are studied in this paper: ZnO and GaN films deposited on R-sapphire and GaN films deposited on (1-100) M-sapphire. Different techniques of epitaxial growth have been used for the fabrication of the films: molecular beam epitaxy for ZnO, metal organic vapor phase epitaxy for GaN on R-sapphire and hybrid vapor phase epitaxy (HVPE) for GaN on M-sapphire. Details of the growth processes are given elsewhere.¹²⁻¹⁴ ZnO and GaN films deposited on R-sapphire always have the nonpolar (11-20) A-orientation whereas the HVPE growth conditions have been chosen to obtain a GaN (1-100) M-orientation on M-sapphire.¹⁵ The epitaxial relationships are represented in Figure 1 and the lattice mismatches are given in Table I.

Cross-sectional (CS) and plane-view (PV) TEM samples were prepared in a classical way by mechanical polishing followed by ion-milling. A very thin (<5 nm) ZnO film has been studied in PV. The preparation of ZnO films is always tricky with possible irradiation damages during ion-milling.⁸ The final step of the ion-milling for this sample (formation of a hole) has been conducted at 1.5 kV in order to avoid the formation of defects and the re-deposition of material on the surface. The observations are made in a JEOL 2010F (200 kV) microscope.

III. STRUCTURAL DEFECTS

We already reported on the nature and densities of structural defects found in (11-20) ZnO⁸ and (11-20) GaN⁶ films grown on R-sapphire. The microstructure of such films is schematically represented in Figure 2. BSFs, which are the defects dominating the microstructure, are nucleated at the interface and thread up to the surface of the films. BSFs are connected to the non-faulted crystal by PDs which have

mainly vertical lines. Two neighbouring BSFs may also be connected by inclined PSFs situated in {11-20} planes. M-GaN films also contain a high density of BSFs, PDs and PSFs. The defect densities in the different films studied are reported in Table II. Different types of BSFs exist in the

TABLE I. In-plane lattice mismatches of nonpolar A-GaN and A-ZnO with R-sapphire and M-GaN with M-sapphire along the 2 main perpendicular in-plane directions. N is the distance between interfacial misfit dislocations necessary for a full relaxation. The densities of misfit dislocations (1/N) along [0001] are also given.

	Orientation	Mismatch	N (nb. of planes)	N (nm)	1/N (10^5 cm^{-1})
A-GaN	\perp [0001]	16.1%	6.2 (1-100) _{GaN}	1.7	
	\parallel [0001]	1.2%	88.7 (0002) _{GaN}	23	4.3
A-ZnO	\perp [0001]	18.3%	5.45 (1-100) _{ZnO}	1.53	
	\parallel [0001]	1.55%	65 (0002) _{ZnO}	16.9	5.9
M-GaN	\perp [0001]	26%	3.8 (11-20) _{GaN}	0.6	
	\parallel [0001]	9%	11 (0002) _{GaN}	2.85	35

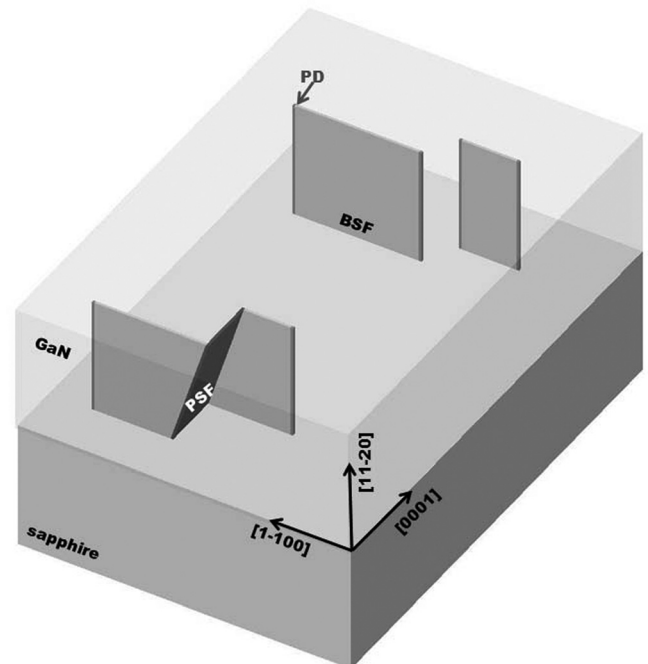


FIG. 2. Schematic representation of structural defects in an A-oriented wurtzite film on R-sapphire. The different kinds of defects are indicated. The wurtzite axes are also shown.

TABLE II. Measured densities of structural defects for A-GaN⁶ and A-ZnO⁸ on R-sapphire and for M-GaN on M-sapphire (this work).

	BSFs (10^5 cm^{-1})	PDs (10^{10} cm^{-2})	PSFs (10^3 cm^{-1})
A-GaN	4-10	9-20	5-20
A-ZnO	1-2	4-7	—
M-GaN	4-5	1-2	Not determined

wurtzite structure, two intrinsic, labelled I_1 and I_2 , and one extrinsic labelled E.¹⁶ All the observed BSFs in the different studied samples are of I_1 type. The displacement vector for I_1 BSF is $1/6 \langle 20\bar{2}3 \rangle$. Note that other kinds of defects may exist in the films (inversion domain boundaries, I_2 BSFs, perfect dislocations). In this paper, we focus only on I_1 BSFs which are dominating the microstructure and which exist in all GaN- and ZnO-based heteroepitaxial nonpolar films. Figure 3 shows high resolution TEM (HRTEM) images of BSFs and their terminating PDs observed in PV taken from ZnO (Figures 3(a) and 3(b)) and GaN (Figure 3(c)) (11–20)-plane films. The widths of BSFs range from a few nano-

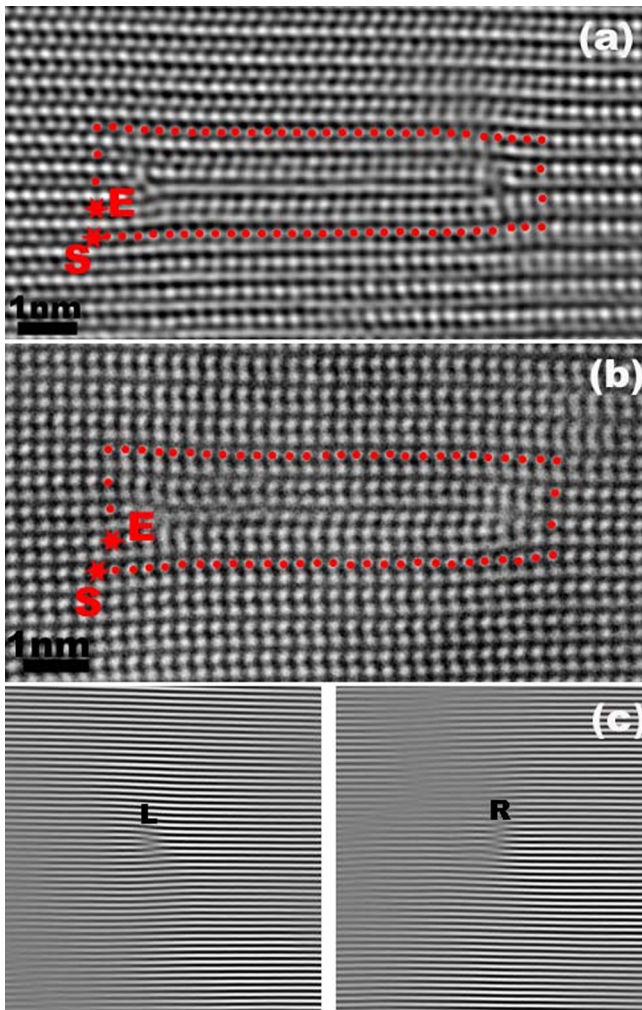


FIG. 3. (a) and (b) PV-HRTEM of BSF in a (11–20) oriented ZnO film. Burger circuits (from S to E) show that the BSF + PD groups correspond to a dissociated c -type dislocation (a) and an $a+c$ -type dislocation (b). (c) PV-(0002) lattice images of the left (L) and right (R) edges of a BSF in a (11–20) oriented GaN film.

meters to several hundred of nanometers in the case of ZnO films and from several tenths of nanometers to several micrometers in the case of GaN films. The BSFs shown in ZnO films are small enough to obtain lattice resolution for the whole area containing the BSFs. Burger circuits drawn around these BSFs reveal that the BSF+PD group in Figure 3(a) corresponds to a c -type dissociated perfect dislocation. This dissociation may be described using c -dislocations and PDs Burger vectors as: $[0001] = 1/6[20\bar{2}3] + 1/6[\bar{2}023]$. This dissociated dislocation may have a non-observable component parallel to the observation direction (an a -component). Therefore, it may result from the dissociation of a $a+c$ -type perfect dislocation. The BSF+PD group in Figure 3(b) corresponds to an $a+c$ -type perfect dislocation, which is dissociated. This dissociation may be described using $a+c$ -dislocations and PD Burger vectors as: $1/3[11\bar{2}3] = 1/6[20\bar{2}3] + 1/6[02\bar{2}3]$. It has to be noted that these 2 kinds of dissociated dislocations have a vertical line and an in-plane edge component. Therefore, they induce in-plane misorientations. In GaN films, it is not possible to obtain lattice resolution at the two ends of BSFs because of their wider lateral size. However, it is possible to image the (0002) planes. Figure 3(c) shows the 2 ends (PDs) of a BSF in a (11–20)-plane GaN film. This BSF corresponds to a missing (0002) plane; the 2 PDs have opposite Burger vector components along the c -direction. Thus, the BSF+PD group does not result from the dissociation of a perfect dislocation with a c -component. It is not possible to conclude if the BSF+PD group is a dislocation with an a -component, because only the (0002) planes can be observed. Actually, from a few tenths of PV-observations in ZnO and in GaN we found:

- BSF+PD groups resulting from the dissociation of perfect dislocations
- BSF+PD groups which do not result from the dissociation of perfect dislocations.

The two configurations have similar densities.

The observation of the dissociation of perfect dislocations may be surprising at the first sight. BSFs may result from the dissociation of perfect dislocation.¹⁶ However, the PDs terminating I_1 BSFs have a Burger vector $(1/6\langle 20\bar{2}3 \rangle)$ with a component out of the basal plane. Therefore, the formation of an I_1 BSF by dissociation of a perfect dislocation requires a climb of PDs which is energetically unfavourable.

It has to be noted that all the observed PDs have vertical lines. Therefore, they have no effect on the relaxation of the mismatch stress.

IV. MECHANISMS OF BASAL STACKING FAULT FORMATION

In this section, we propose several possible mechanisms for the formation of BSFs in nonpolar wurtzite. Then we try to determine which one mainly occurs in nonpolar wurtzite heteroepitaxial films growth. First, let us consider the formation energy of BSFs. The different BSFs, I_1 , I_2 , and E, can be described as the introduction of respectively one, two and three cubic stacks in the hexagonal wurtzite structure.

The formation energy of BSFs is directly related to the number of cubic stacks and calculations confirm that the observed I_1 BSFs have the lowest formation energy.^{17,18}

A. Classical mechanisms

Two formation mechanisms of BSFs are classically presented in the literature: they result either from growth errors¹⁹ or from the condensation of vacancies.¹⁶ Growth errors occur when adatoms are deposited in a wrong position (a cubic position in the case of a hexagonal stacking). If the surface diffusion of the adatoms is sufficiently high, the probability of forming growth errors is low. When GaN and ZnO are grown along the c -direction (polar orientation), BSFs are rarely observed. In fact, for GaN, BSFs are only reported for nucleation layers which are grown far below the optimum growth temperature²⁰ or when the growth is performed along the $-c$ -direction like in nonpolar GaN epitaxial lateral overgrown (ELO) films.^{21,22} For ZnO, whatever the polarity of the growth ($+c$ or $-c$), BSFs are rarely observed. In fact, BSFs in ZnO films are only observed for irradiated materials²³ in which the density of point defects is very high. The growth conditions are similar for polar and nonpolar orientations therefore the adatoms diffusion length and point defects concentration are also similar. These classical mechanisms can be only invoked in the case of GaN for a 3D-growth with islands exhibiting $-c$ -facets. As BSFs exist with similar densities in GaN and ZnO films, these mechanisms are likely not the predominant ones.

B. Mismatch relaxation

In heteroepitaxial growth, structural defects are often introduced to relax the stress due to the difference of lattice parameters between the deposited layer and the substrate. In this section, a scenario where BSFs are introduced for lattice mismatch relaxation is considered.

A local variation of the stacking does not significantly change the interatomic distances therefore a BSF has no noticeable influence on the relaxation of misfit stress. On the other hand, the termination of a BSF in an interface may have an effect on the misfit strain relaxation by helping the formation of misfit dislocations (MDs). As the densities of MDs are similar or higher than the densities of BSFs, such a mechanism of BSF formation has been proposed for nonpolar GaN films on sapphire.²⁴ The in-plane densities of MDs necessary for a full relaxation of the films along $[0001]$ are given in Table I. In the case of fully wurtzite heterostructures grown along M -orientation, the relaxation of the stress by the formation of either I_1 (InGaN/GaN)²⁵ or I_1 and I_2 BSFs (GaN/AlN/GaN)²⁶ has been reported. In these cases, the PDs terminating the BSFs have their line and an edge component in the interfacial plane and are in fact MDs, BSFs corresponding to either extra- or missing half-planes. The situation is more complex in the case of the growth on sapphire substrate which has a structure which is very different from the wurtzite one. The interfacial structure is, of course, different at the termination of a BSF than below a non-faulted wurtzite region. But it is not obvious that this special configuration of the interfacial structure corresponds to a MD. It is

difficult to experimentally study that in the case of $(11\text{--}20)$ -oriented films. In fact, MDs are observed in CS along the $[1\text{--}100]$ zone axis but in this case BSFs are out-of-contrast. BSFs are observed along the $[2\text{--}1\text{--}10]$ zone axis which is inclined by 30° from the CS orientation (see Figure 1). In this orientation, an interfacial region corresponding to the superposition of the substrate and the epilayer is observed and MDs are not revealed.⁶ The situation is easier to analyse in the case of $(1\text{--}100)$ M -oriented films. Figure 4(a) is a CS-HRTEM image of the interfacial region between M -GaN and M -sapphire along the $[11\text{--}20]_{\text{GaN}}$ ($[0001]_{\text{sapphire}}$) zone axis which is in the growth plane. Both MDs and BSFs are observed along this zone axis. Figure 4(b) shows the spots used for Fourier filtering: MDs are seen on the Fourier filtered image of Figure 4(a) using the $(0002)_{\text{GaN}}$ and $(11\text{--}20)_{\text{sapphire}}$ spots (Figure 4(c)), whereas BSFs are seen in the Fourier filtered image of Figure 4(a) using the $(1\text{--}100)_{\text{GaN}}$ (Figure 4(d)). Most of the MDs and BSFs are situated at positions differing of several $(0002)_{\text{ZnO}}$ atomic planes. We have carefully acquired the HRTEM images at a focus close to the minimum contrast in order to limit the delocalization phenomena. The separation between the positions of MDs and BSFs is therefore real. From this observation, it can be concluded that the main origin of BSF is not related to the relaxation of the misfit strain. This result may reasonably be extended to $(11\text{--}20)$ -oriented films as the density of BSFs is similar and the densities of MDs lower.

C. Coalescence of nuclei

Another invoked origin of the BSFs is that they result from the coalescence of nuclei at the very first stages of the growth.^{8,27} To verify this hypothesis, we studied a very thin (≤ 5 nm) $(11\text{--}20)$ ZnO film in plane-view orientation. The normal to the film surface is $[11\text{--}20]_{\text{ZnO}}$ but this direction is not a principal axis of the sapphire structure.²⁸ In the selected area diffraction pattern in PV orientation (insert in Figure 5), $(1\text{--}100)_{\text{ZnO}}$ and $(11\text{--}20)_{\text{sapphire}}$ diffraction spots are visible along one in-plane orientation whereas only the $(0002)_{\text{ZnO}}$ spot is visible along the perpendicular in-plane direction. Figure 5 also shows a PV dark field image using the $(1\text{--}100)_{\text{ZnO}}$ and $(11\text{--}20)_{\text{sapphire}}$ diffraction spots. The main contrasts observed in Figure 5 are translational moiré fringes resulting from the overlapping of the $(1\text{--}100)_{\text{ZnO}}$ and $(11\text{--}20)_{\text{sapphire}}$ planes with different interplanar spacings. These contrasts are not observed everywhere in the image. The regions without moiré pattern fringes correspond to uncovered sapphire. Therefore, at this early stage of the growth, the epilayer is not continuous and is formed of islands slightly elongated along the $[1\text{--}100]_{\text{ZnO}}$ direction. The typical sizes of these nuclei are 20–50 nm along $[1\text{--}100]_{\text{ZnO}}$ and 5–10 nm along $[0001]_{\text{ZnO}}$. The period of the moiré fringes (≈ 1.53 nm) corresponds to a full relaxation of the mismatch along the $[1\text{--}100]_{\text{ZnO}}$ direction (see Table I). Along this in-plane direction the mismatch is large and the relaxation occurs following the domain matching epitaxy model (DME)²⁹ with the matching of n planes of ZnO with $n+1$ planes of sapphire.³⁰ The terminations of extra half-planes in the interface are defined as “geometrical MDs.”³¹

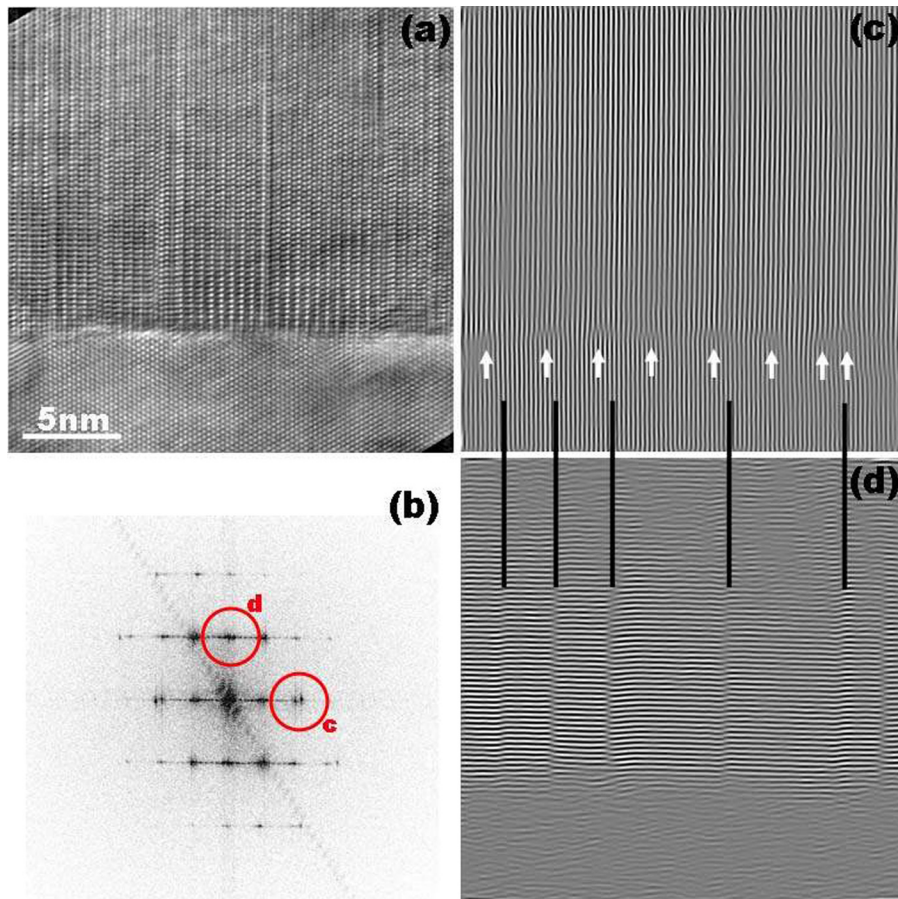


FIG. 4. (a) HRTEM image of the interface between (1-100) GaN and M-sapphire along the $[11-20]_{\text{GaN}}$ ($[0001]_{\text{sapphire}}$) zone axis. (b) Fourier transform of the image in Figure 2(a). The spots used for Fourier filtering in Figures 2(c) and 2(d) are indicated. (c) Fourier filtered image of the image in Figure 2(a) using $(0002)_{\text{GaN}}$ and $(11-20)_{\text{sapphire}}$ spots. The white arrows indicate additional planes in sapphire (MD). (d) Fourier filtered image of the image in Figure 2(a) using $(1-100)_{\text{GaN}}$ spot. The black lines indicate the positions of BSFs.

The same mode of relaxation has also been observed for A-GaN grown on R-sapphire.³² As only the $(0002)_{\text{ZnO}}$ diffraction spot is visible in the perpendicular $[0001]_{\text{ZnO}}$ direction, we have no information on the strain along this direction. Cross section observation of thick ZnO films reveals the presence of a residual compressive strain.³⁰ The islands observed in the studied thin film should therefore only be partially relaxed along the $[0001]$ direction. A few defects

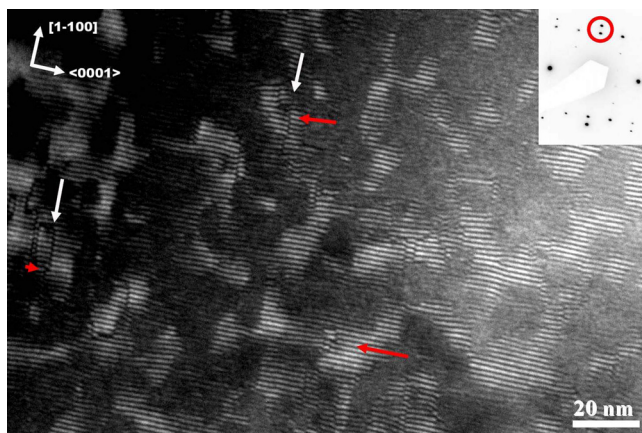


FIG. 5. PV-dark field image of a thin layer (a few nanometers) of (11-20) ZnO on R-sapphire. The inset is a selected area electron diffraction pattern where the $(1-100)_{\text{ZnO}}$ and $(11-20)_{\text{sapphire}}$ spots used for imaging are shown. White arrows indicate BSFs and red arrows edge dislocations. The ZnO axes are indicated.

are observed in the moiré fringe lattice, either a translation of the fringes (white arrows) or an additional fringe (red arrows). These two kinds of defects may be also observed mixed (white + red arrows). The sapphire substrate being of high crystalline quality, these defects are defects in the ZnO islands. The translations of the moiré fringes may correspond to BSFs, while the additional fringes to vertical edge dislocations, as already suggested by the PV-observations of c-oriented AlN films on sapphire.³³ The mixed defects (translation + additional plane) may correspond to BSF+PD groups with a dissociated dislocation character. It has to be noted that a lot of islands are free of any defect.

PV-HRTEM has been performed in order to have a better insight in the structure of the ZnO initial islands (Figure 6(a)). Three regions are labelled, regions 1 and 2 being associated with one nucleation island and region 3 to another neighbouring island. Figure 6(b) is a Fourier filtered image using the $(1-100)_{\text{ZnO}}$ spot which clearly highlights a translation of the planes between region 1 and 2 (white arrows). The boundary between regions 1 and 2 is formed of 2 linear segment parallel to $(0002)_{\text{ZnO}}$ planes and which correspond to BSFs. The connection between the 2 BSFs should correspond to a PSF. The HRTEM image has also been analysed using geometrical phase analysis (GPA).³⁴ Figure 7(a) is a phase image using the $(1-100)_{\text{ZnO}}$ in-plane spatial frequencies of the HRTEM image of Figure 6(a). The phase is equal, in each point i , to $-2\pi\mathbf{g}\cdot\mathbf{r}(i)$, \mathbf{g} being the lattice planes considered and \mathbf{r} the displacement of the planes from their

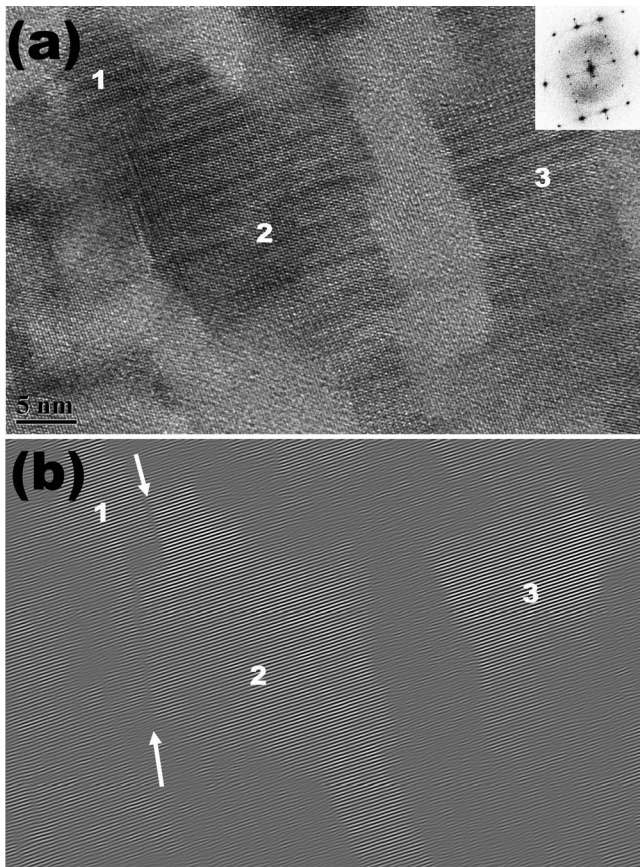


FIG. 6. (a) PV-HRTEM image of a thin (a few nanometers) (11–20) ZnO on R-sapphire. The inset is the Fourier transform. (b) Fourier filtered image of the image in Figure 4(a) using the $(1-100)_{\text{ZnO}}$ spot. White arrows indicate BSFs.

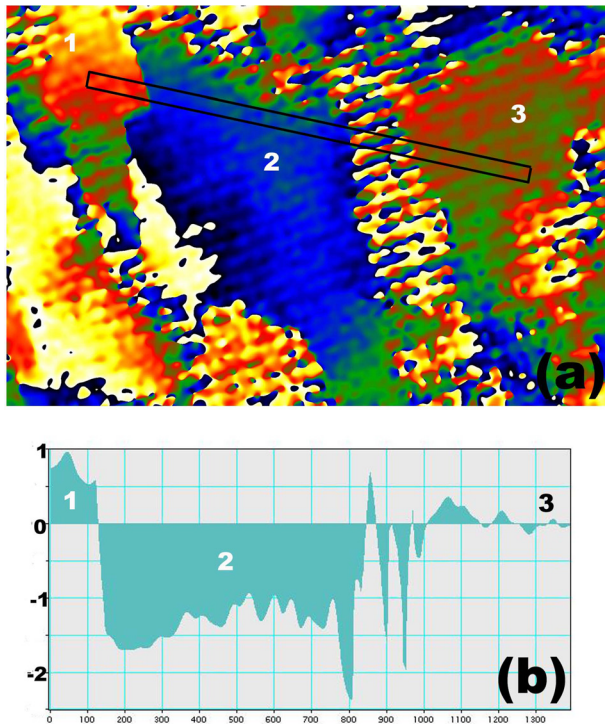


FIG. 7. (a) Phase image of the image in Figure 6(a) for $(1-100)_{\text{ZnO}}$ planes. The phase reference is in region 3. (b) Profile of the phase in the rectangle drawn in Figure 7(a), the intensities being projected along the small side of the rectangle.

reference position. The contrasts are almost homogeneous in regions 1, 2, and 3 but different between the different regions. A phase difference can be due to a difference of lattice parameters, to a rotation or to a translation of the lattice. Neither difference of lattice parameter nor rotation of the lattice has been measured by GPA therefore the contrast difference is due to a translation of the $(1-100)$ planes. Figure 7(b) is an intensity profile taken from Figure 7(a) in the drawn rectangle (projection of the intensities along the small side of the rectangle). A phase difference of about 2 is observed between regions 1 and 2, which is consistent with the translation of an I_1 BSF ($2\pi \cdot g \cdot R = 2\pi/3 = 2.09$). A phase difference and therefore a translation of the lattice is also observed between uncoalesced regions 2 and 3. Here again, the HRTEM images have been carefully acquired at a focus close to the minimum contrast. Therefore, such a translation between uncoalesced islands is real. Moreover, as it will be discussed in Sec. V, such a translation is expected in the case of a 3D-growth mode with large lattice mismatches. The formation of BSFs may occur when two of such translated growth islands coalesce. With the observed high density of growth islands, the formation of BSFs at coalescence boundaries is certainly their predominant mechanism of formation. This mechanism is discussed in Sec. V.

V. DISCUSSION

Because of the large structural and chemical differences, the interfacial energies between wurtzite materials and sapphire substrates are high resulting in a Volmer-Weber growth mode whatever the orientation. Moreover, the large difference in the lattice parameters, at least along one in-plane direction, is accommodated by the formation of geometrical MDs. These interface dislocations are formed at the very beginning of the growth without the necessity of standard plastic relaxation mechanisms including dislocation glide.³⁵ The initial islands are therefore free of threading defects. The MDs are nucleated independently in the different islands therefore the probability that the geometrical MDs correspond to the same plane in the different islands is low. This probability is $1/(n+1)$ for a matching of n planes of the epilayer with $n+1$ planes of the substrate (or $n+1$ planes of the epilayer with n planes of the substrate). It has to be noted that this probability increases with the mismatch, the maximum value being $1/2$ for a mismatch of 50%. In the case of $(11-20)$ ZnO on R-sapphire, a matching of 5 $(1-100)$ wurtzite planes with 6 $(11-20)$ sapphire planes has been chosen since a ratio of 5.45/6 ratio has been measured.³⁰ This configuration is schematically represented in Figure 8(a). The $(1-100)$ wurtzite planes are shown in red while the $(11-20)$ sapphire planes are marked in blue. Geometrical MDs (extra half plane) in the sapphire substrate are shown by black arrows. Two independent islands with an arbitrary rectangle shape are represented. The geometrical MDs at the interface of the two islands with the substrate do not correspond to the same sapphire planes. The independent nucleation of MDs in different islands results in high probability $(n/(n+1))$ of the existence of a translation of the lattice planes between different islands. A coalescence of islands

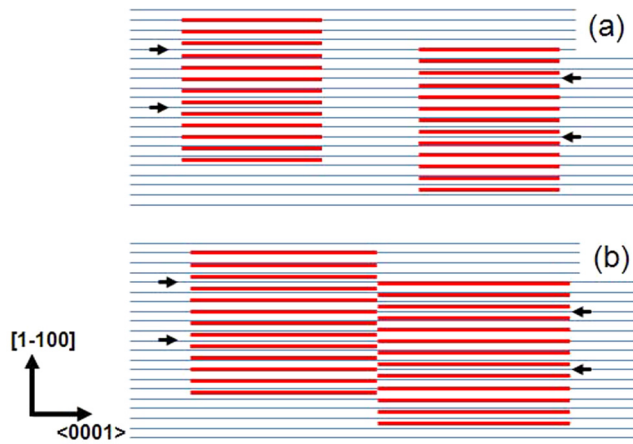


FIG. 8. (a) Schematic representation of the initial stage of the nucleation of (11-20) ZnO on R-sapphire. The sapphire (11-20) planes are represented in blue and the ZnO (1-100) planes in red. The black arrows indicate geometrical MDs. Two independent growth islands are shown. The crystalline directions of ZnO are indicated. (b) Coalescence of the two islands of Figure 8(a). The independent formation of geometrical MDs in the two islands result in a translation of the (1-100)_{ZnO} planes.

with a translation of atomic planes is represented in Figure 8(b).

Several mechanisms for compensating such a translation may be suggested. First, the translation may be compensated by a simple elastic strain of the atomic planes. Second, the translation may be compensated by the formation of crystalline defects. The ability of crystalline defects to compensate a translation of atomic planes between coalescing islands depends on some of their parameters. For a dislocation, its Burger vector has to be compared to the translation vector. For a planar defect, its displacement vector has also to be compared to the translation vector but, moreover, the angle between the plane of the defect and the coalescence boundary has to be taken into account. And obviously, whatever the defect is, its associated strain and its formation energy have to be taken into account.

We will now consider two types of defects, intrinsic BSFs (I_1 and I_2) and perfect dislocations for the compensation of translation of (1-100) planes in the case of nonpolar A-oriented wurtzite films. For nonpolar orientations, BSFs are perpendicular to the horizontal growth plane. In the studied case of ZnO on R-sapphire, the growth islands exhibit facets close to a {0001} orientation, that are therefore similar to the plane of BSFs (see Figure 5). Considering the displacement fields of the defect, both I_1 and I_2 BSFs have displacement vectors with a component in the growth planes along [1-100] (I_2 displacement vector = $1/3\langle 10-10 \rangle$). A residual strain may subsist because the probability to match perfectly the translation between islands with the displacement vector of a BSF is low. Both a - and $a+c$ -type perfect dislocations also have an in-plane component along [1-100]. And they can have a line in the coalescence boundary. Therefore intrinsic BSFs and perfect dislocations should have a similar efficiency for compensating the translations between islands. It has to be noted that I_1 BSFs have a displacement vector with a component parallel to the translation direction but also a component perpendicular to the transla-

tion direction whereas I_2 BSFs have only a component parallel to the translation direction. The fact that we mainly observed I_1 BSFs should be related to their lower associated strain and formation energy as compared to the associated strain and formation energies of I_2 BSFs and perfect dislocations. Moreover, the compensation of translation by only elastic strain should not be energetically favourable.

Perfect dislocations are also sometimes observed linked to an I_1 BSF. These perfect dislocations are either c - or $a+c$ -type dislocations, i.e., with a component perpendicular to the basal plane. Such a component has no effect for compensating the translations of [1-100] planes. We assume that such dislocations are introduced to compensate possible in-plane misorientations between adjacent islands.

A similar mechanism of defect formation may be proposed for any other nonpolar orientations. In the case of M-oriented films, the translation of (11-20) planes between growth islands may also be compensated by I_1 BSFs even if their component in the basal plane is not parallel to the translation between islands.

For polar orientations, BSFs are parallel to the growth surface (perpendicular to the coalescence boundaries) and are therefore not efficient for compensating translations between growth islands. In this case, perfect dislocations are introduced in the coalescence boundaries between the nuclei formed at the early stage of the nucleation layer growth.³³ The situation is intermediate in the case of semipolar orientations with inclined (0001) planes. Indeed, perfect dislocations have been detected in semipolar (11-22)-oriented GaN together with BSFs³⁶ while only BSFs are observed in nonpolar GaN films.

The mechanism of defect formation that we described here-above is closely related to a 3D nucleation. On the other hand, growth processes including a 3D growth stage are often used to reduce the density of defects especially in the case of GaN films deposited on sapphire in both polar³⁷ and nonpolar³⁸ orientations. By tuning the growth conditions, a transition from 3D to 2D growth modes allows eventually obtaining flat films. However, distinction should be made between these 3D growth processes and a 3D nucleation. In the case of a 3D growth process, large islands are formed after an annealing of a continuous nucleation layer. This nucleation layer may have been formed by a mechanism of 3D nucleation. Large islands already contain structural defects, dislocations in the case of polar growth and BSFs in the case of nonpolar growth. The final microstructure of micrometer thick GaN polar films results from the movement of dislocations.³⁹ On the other hand, BSFs are confined in the basal planes and it can be assumed that their distribution in nonpolar films does not significantly change with the thickness of the deposited film. The final microstructure of nonpolar film is therefore mainly determined by the initial 3D nucleation.

VI. CONCLUSION

Different mechanisms explaining the formation of BSFs in nonpolar wurtzite films deposited on highly dissimilar sapphire substrates have been proposed and evaluated. From our experimental observations, we conclude that the

mechanisms related to growth errors, to condensation of point defects or to the relaxation of mismatch stress are not the main ones. Our TEM investigations of a very thin sample (nucleation stage) show that the BSFs are mainly introduced at the coalescence of 3D nuclei to compensate a translation of lattice planes. This translation is due to the presence of misfit dislocations independently introduced in neighboring islands at the substrate interface.

In the case of nonpolar films, I_1 BSFs are well-adapted for compensating such a translation. Their plane is similar to the coalescence plane and they have a component of their displacement vector parallel to the direction of translation. Moreover, their formation energy is low so they are likely to occur easily.

A 3D nucleation (Volmer Weber growth mode) is expected in the case of any heteroepitaxy on highly dissimilar substrates. The same mechanism may therefore be proposed to explain the formation of BSFs in nonpolar wurtzite films deposited on other highly dissimilar substrates with large lattice mismatches.

The ability of BSFs to compensate translations of planes between neighbouring nuclei decreases with the increase of the angle between their plane (the basal plane) and the coalescence plane, i.e., from nonpolar to polar orientations. This remark is in agreement with experimental observations of a decrease of BSF densities from nonpolar to polar orientations with semipolar orientations being intermediate cases.

With such a formation mechanism, the density of BSFs in nonpolar films is clearly related to the density of nuclei. It is therefore certainly possible to play with the growth conditions in order to reduce the BSF density. However, to obtain a 2D layer of a reasonable thickness, the nuclei density should not be reduced too much. Therefore, the formation of BSFs seems to be intrinsic to the heteroepitaxial growth of wurtzite materials along nonpolar orientations on highly dissimilar substrates.

ACKNOWLEDGMENTS

E. Beraudo (CRHEA) is acknowledged for his assistance in the construction of the figures. M. Leroux (CRHEA) and B. Vinter (University of Nice) are also acknowledged for a critical reading of the manuscript.

¹F. Nye, *Physical Properties of Crystals* (Clarendon, Oxford, 1957).

²J. S. Speck and S. F. Chichibu, *MRS Bull.* **34**, 304 (2009).

³M. Horita, J. Suda, and T. Kimoto, *Appl. Phys. Lett.* **89**, 112117 (2006).

⁴N. Onojima, J. Suda, T. Kimoto, and H. Matsumi, *Appl. Phys. Lett.* **83**, 5208 (2003).

⁵M. D. Craven, S. H. Lim, F. Wu, J. S. Speck, and S. P. DenBaars, *Appl. Phys. Lett.* **81**, 469 (2002).

⁶P. Vennéguès, F. Mathal, and Z. Bougrioua, *Phys. Status Solidi C* **3/6**, 1658–1661 (2006).

⁷T. Y. Liu, A. Trampert, Y. J. Sun, O. Brandt, and K. H. Ploog, *Philos. Mag. Lett.* **84**, 435 (2004).

⁸P. Vennéguès, J. M. Chauveau, M. Korytov, C. Deparis, J. Zúñiga-Pérez, and C. Morhain, *J. Appl. Phys.* **103**, 083525 (2008).

⁹J. W. Lee, S. K. Han, S. K. Hon, J. Y. Lee, and T. Yao, *J. Cryst. Growth* **310**, 4102 (2008).

¹⁰S.-H. Lim and D. Shindo, *J. Appl. Phys.* **88**, 5107 (2000).

¹¹P. Vennéguès, S. Founta, H. Mariette, and B. Daudin, *Jpn. J. Appl. Phys. Part 1* **49**, 040201 (2010).

¹²J.-M. Chauveau, D. Buell, B. Vinter, M. Lügt, P. Vennéguès, M. Teysère-Donnelli, S. Bérard-Bergery, C. Deparis, and C. Morhain, *J. Cryst. Growth* **301**, 366 (2007).

¹³Z. Bougrioua, M. Lügt, P. Vennéguès, I. Cestier, T. Günhe, E. Frayssinet, P. Gibart, and M. Leroux, *Phys. Status Solidi A* **204**(1), 282–289 (2007).

¹⁴T. Zhu, D. Martin, and N. Grandjean, *Jpn. J. Appl. Phys., Part 1* **48**, 020226 (2009).

¹⁵P. Vennéguès, T. Zhu, D. Martin, and N. Grandjean, *J. Appl. Phys.* **108**, 113521 (2010).

¹⁶D. Hull and D. J. Bacon, *Introduction to Dislocations*, 4th ed. (Butterworth-Heinemann, Oxford, 2001).

¹⁷Y. Yan, G. M. Dalpian, M. M. Al-Jassim, and Su-Huai Wei, *Phys. Rev. B* **70**, 193206 (2004).

¹⁸C. Stampfl and C. G. Van de Walle, *Phys. Rev. B* **57**, R15052 (1998).

¹⁹F. Ernst and P. Pirouz, *J. Mater. Res.* **4**, 834 (1989).

²⁰P. Vennéguès, B. Beaumont, M. Vaille, and P. Gibart, *J. Cryst. Growth* **173**, 249 (1997).

²¹F. Wu, M. D. Craven, S.-H. Lim, and J. S. Speck, *J. Appl. Phys.* **94**, 942 (2003).

²²T. Günhe, M. Albrecht, Z. Bougrioua, P. Vennéguès, and M. Leroux, *J. Appl. Phys.* **101**, 113101 (2007).

²³J. Couderc, *Microsc. Microanal. Microstruct.* **6**, 229 (1995).

²⁴J. Smalc-Koziorowska, G. Tsiakatouras, A. Lotsari, A. Georgakilas, and G. P. Dimitrakopoulos, *J. Appl. Phys.* **107**, 073525 (2010).

²⁵F. Wu, Y. D. Lin, A. Chakraborty, H. Ohta, S. P. Den Baars, S. Nakamura, and J. S. Speck, *Appl. Phys. Lett.* **96**, 231912 (2010).

²⁶J. Smalc-Koziorowska, M. Sawicka, T. Remmele, C. Skierbiszewski, I. Grzegory, and M. Albrecht, *Appl. Phys. Lett.* **99**, 061901 (2011).

²⁷A. Trampert, T. Y. Liu, O. Brandt, and K. H. Ploog, *J. Phys. IV* **132**, 221 (2006).

²⁸J. W. Lee, S. K. Han, S. Hong, and J. Y. Lee, *Appl. Surf. Sci.* **256**, 1849 (2010).

²⁹J. Narayan and B. C. Larson, *J. Appl. Phys.* **93**, 278 (2003).

³⁰J.-M. Chauveau, P. Vennéguès, M. Lügt, C. Deparis, J. Zuniga-Perez, and C. Morhain, *J. Appl. Phys.* **104**, 073535 (2008).

³¹Y. Ikuhara, P. Pirouz, A. H. Heuer, S. Yadavalli, and C. P. Flynn, *Philos. Mag. A* **70**, 75 (1994).

³²P. Vennéguès and Z. Bougrioua, *Appl. Phys. Lett.* **89**, 111915 (2006).

³³Th. Kehagias, Ph. Komninou, G. Nouet, P. Ruterana, and Th. Karakostas, *Phys. Rev. B* **64**, 195329 (2001).

³⁴M. J. Hÿtch, E. Snoek, and R. Kilaas, *Ultramicroscopy* **74**, 131 (1998).

³⁵G. Saint-Girons, J. Cheng, P. Régreny, L. Largeau, G. Patriarche, and G. Hollinger, *Phys. Rev. B* **80**, 155308 (2009).

³⁶P. Vennéguès, Z. Bougrioua, and T. Günhe, *Jpn. J. Appl. Phys. Part 1* **46**(7A), 4089 (2007).

³⁷P. Vennéguès, B. Beaumont, S. Haffouz, M. Vaille, and P. Gibart, *J. Cryst. Growth* **187**, 167 (1998).

³⁸C. J. Johnston, M. J. Kappers, and C. J. Humphreys, *J. Appl. Phys.* **105**, 073102 (2009).

³⁹M. A. Moram, C. S. Ghedia, D. V. S. Rao, J. S. Barnard, Y. Zhang, M. J. Kappers, and C. J. Humphreys, *J. Appl. Phys.* **106**, 073513 (2009).